RSC Advances

PAPER

View Article Online
View Journal | View Issue

Cite this: *RSC Adv.*, 2024, **14**, 37598

Ethanol-assisted *in situ* stimulated graphene oxide as support for CuO/NiO nanoparticles†

Manash J. Baruah, ‡[a] Eramoni Saikia,‡[b] Nand Kishor Gour, [c] N. Priyanshu Singh,[b] Bitupon Borthakur, [b] Uttam Mohan,[d] Arup Jyoti Das, [e] Rahul Kemprai,[f] Bikash K. Sarmah,[g] Rupjyoti Dutta,[hi] Young-Bin Park,[j] Biraj Das *[b] and Mukesh Sharma *[f]

Received 12th June 2024
Accepted 14th November 2024

DOI: 10.1039/d4ra04308a

rsc.li/rsc-advances

Herein we report the first successful synthesis of ethanol-assisted *in situ* generated reduced graphene oxide as a support for CuO/NiO nanoparticles. Through the strategic incorporation of Cu and Ni precursors into ethanol, followed by thermal treatment, we achieved the fabrication of reduced graphene oxide-supported CuO/NiO nanoparticles. The material underwent thorough characterization using FT-IR, XRD, TEM, XPS, Raman, and UV-DRS analysis. This method promises a breakthrough approach unveiling an unparalleled potential leading to paradigm shifts in graphene oxide synthesis. A theoretical study has also been performed in support of GO formation from ethanol. The synthesized CuO/NiO nanoparticles over reduced graphene oxide were found to be effective for the reduction of 4-nitrophenol within 5 min.

Introduction

The synthesis of graphene oxide (GO) remains an active and dynamic field of research, propelling advancements across materials science, chemistry, and nanotechnology.[1–5] Through the exploration of novel synthesis techniques and deepening understanding of the underlying processes governing GO formation, researchers are poised to uncover new applications and refine existing ones, fostering innovation across diverse disciplines.[1–5] Particularly noteworthy is the fusion of transition metal oxides nanoparticles (NPs) with GO, presenting a fertile ground for exploration given their distinctive properties and promising applications spanning catalysis, energy storage, and sensing.[6–8] However, the preparation of GO presents inherent challenges owing to the intricate nature of graphite and the targeted functionalization required.[3–5,9,10] Overcoming these hurdles is pivotal for harnessing the exceptional properties and wide-ranging applications of graphene-based materials. Therefore, concerted efforts to develop efficient, scalable, and reproducible synthesis methods are indispensable for fully realizing the potential of graphene oxide in various technological and scientific domains.

Several methods have been developed for the preparation of graphene oxide (GO), and reduced graphene oxide (rGO) each offering distinct advantages regarding scalability, reproducibility, and control over material properties.[11–16] Prominent methods include the Hummers' method, and the Staudenmaier method.[11,12] A comparative table showcasing different approach for GO synthesis is provided in Table S1.† However, the Hummers and Staudenmaier methods, despite their widespread adoption, come with drawbacks such as safety concerns due to the use of strong acids, potential environmental risks, and the necessity for careful handling of hazardous chemicals.[11,12] These challenges underscore the need for alternative approaches each with its own set of advantages and limitations.

[a]*Department of Chemistry, D. C. B. Girls College, Jorhat, Assam, India, 785001. E-mail: manashjbom@gmail.com*

[b]*Department of Chemistry, D. D. R. College, Chabua, Dibrugarh, Assam, India, 786184. E-mail: eramonisaikia@gmail.com; birajdaschm@gmail.com; npriyanshusingh27@gmail.com; bituponborthakur@gmail.com*

[c]*Department of Chemical Sciences, Tezpur University, Napaam, Tezpur, Assam, India, 784028. E-mail: nkgour1@tezu.ernet.in*

[d]*Department of Chemistry, D. H. S. K. College, Dibrugarh, Assam, India, 786001. E-mail: uttamohan@rediffmail.com*

[e]*Department of Chemistry, Indian Institute of Technology, Kanpur, India, 208016. E-mail: arupjyoti1994@gmail.com; mcotton233@gmail.com*

[f]*Department of Chemistry, Suren Das College, Hajo, Kamrup, Assam, India, 781102. E-mail: rahulkemprai827@gmail.com*

[g]*Department of Chemistry, Sonari College, Sonari, Charaideo, Assam, India, 785690. E-mail: bikashsarmah93@gmail.com*

[h]*CSIR-North East Institute of Science and Technology, Jorhat, Assam, India, 785006. E-mail: rjydutta@gmail.com*

[i]*Academy of Scientific and Innovative Research (AcSIR), Ghaziabad, India, 201002*

[j]*Department of Mechanical Engineering, Ulsan National Institute of Science and Technology, UNIST-gil 50, Ulju-gun, Ulsan 44919, Republic of Korea. E-mail: ypark@unist.ac.kr*

† Electronic supplementary information (ESI) available: Physical measurements of the physicochemical and spectrochemical tools, comparative table outlining different synthetic routes for rGO along with their preparation methods, BET isotherm, PSD analysis, computational details, a detailed comparison was conducted with the performance of other reported bimetallic CuO/NiO catalysts and catalytic studies of synthesized CuO/NiO/rGO nanocomposite in reduction of 4-NP. See DOI: https://doi.org/10.1039/d4ra04308a

‡ Both the authors have equal contribution.

Ethanol acts as both a solvent and a template, stabilizing the dispersion of GO and the metal precursors. Additionally, it serves as a mild reducing agent, facilitating the reduction of GO to rGO, enhancing the composite's electrical conductivity, and improving the interaction between the NPs and the graphene matrix. Several previous studies also support the role of ethanol as reducing agent. Huba *et al.* reported the role of ethanol as reducing agent for Co and Ni NPs.[17] Recently, Zhao *et al.* also reported the role of ethanol as reducing agent for cobalt-based lithium-ion battery cathodes.[18] Ethanol as solvent is generally considered safer and environmentally friendly than many traditional solvents. Furthermore, since the synthesis process was conducted in the solid state, as a result it enhances the sustainability of the synthesis process and minimizes environmental impact.

Researchers are constantly seeking innovative techniques to enhance the quality, scalability, and functionalization of GO and rGO for diverse applications.[19] Recent advancements in metal oxide-based GO and rGO synthesis encompass various methods such as green synthesis, microwave-assisted synthesis, hydrothermal and solvothermal methods, and bottom-up approaches.[20–23] However, as of now, there is no documented instance of ethanol serving as a template for the design of rGO to support CuO/NiO NPs. Given the significance of rGO synthesis, we present the pioneering method for ethanol-assisted rGO synthesis as a support for CuO/NiO NPs, CuO/NiO/rGO.

Experimental section

Synthesis of CuO/NiO/rGO

To synthesize CuO/NiO/rGO, 14.4 mg of nickel chloride ($NiCl_2 \cdot 2H_2O$) was dissolved in 100 mL of an ethanol/water mixture. A concentrated solution of sodium hydroxide (NaOH) was added until complete precipitation of nickel hydroxide $Ni(OH)_2$ occurred. The precipitate was washed several times with hot water and dried in an oven. The dried $Ni(OH)_2$ was then mixed with 7.5 mg of copper chloride ($CuCl_2$) in a mortar and pestle for 30 hours. The resulting mixture was washed repeatedly with hot water to remove impurities and subsequently dried in an oven at 100 °C to obtain the final GO composites. To promote the interactions between CuO and NiO NPs over the graphitic support, a thermal treatment was carried out at 100 °C for 1 hour, repeated over 30 cycles. A general graphic depiction for the synthesis of the CuO/NiO/rGO is provided in Scheme 1.

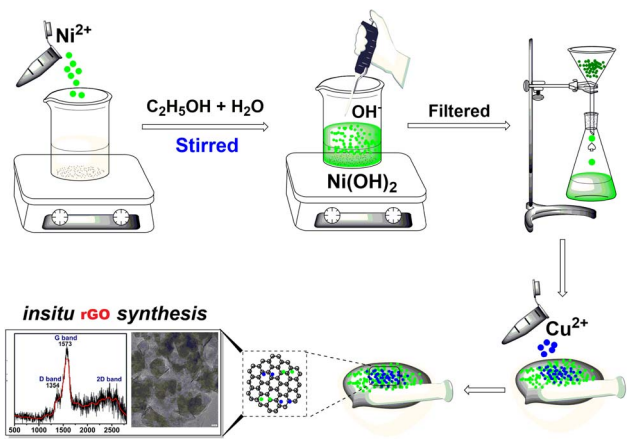

Scheme 1 A pictorial representation for the synthesis of CuO/NiO/rGO.

Procedure for the conversion of 4-nitrophenol (4-NP) to 4-aminophenol (4-AP) using CuO/NiO/rGO

A 0.001 M solution of 4-NP was carefully prepared by dissolving 0.1391 g in 100 mL of water. The reduction process was tracked using UV-vis spectroscopy, with $NaBH_4$ acting as the reducing agent (prepared by dissolving 50 mg in 15 mL of water). To acquire the spectra, 3 mL of the 4-NP solution was added to a cuvette containing 8 mg of CuO/NiO/rGO catalyst followed by the dropwise addition of 200 μL of $NaBH_4$.

Results and discussion

Comprehensive characterization using X-ray diffraction (XRD), Fourier-transform infrared spectroscopy (FT-IR), UV-visible diffuse reflectance spectroscopy (UV-DRS), Transmission Electron Microscopy (TEM), Raman spectroscopy, and X-ray photoelectron spectroscopy (XPS) revealed detailed insights into the composition and structure of synthesized CuO/NiO/rGO. The XRD analysis showed characteristic peaks at 12.8°, 19.2°, and 26.2° corresponding to rGO sheets, with the (001) peak at 12.8° indicating highly intercalated oxide functional groups.[24] Additionally, sharp peaks were observed for CuO (JCPDS no. 48-1548) at 32.6° (110), 38.7° (111), 50.4° (202), 53.8° (020), 62.3° (113), and 68° (220), and for NiO (JCPDS no. 04-0835) at 38.7° (111), 44.6° (200), 62.3° (220), and 76.5° (222), suggesting the co-existence of oxide phases in Fig. 1a.[25–28] Minor shifts in the XRD peaks could be attributed to the interaction between the metal oxides and the rGO template.

The FT-IR spectra further inveterate the chemical structure of CuO/NiO/rGO, identifying a strong peak at 1724 cm^{-1} for C=O stretching, an O–H deformation at 1405 cm^{-1}, and a peak at 1620 cm^{-1} for graphitic skeletal vibrations, Fig. 1b.[24,29,30] The weakening of peak intensity at 1724 cm^{-1} indeed suggests the conversion of graphene oxide (GO) to reduced graphene oxide (rGO) during the synthesis process.[31] Vibrational bands at 463 cm^{-1} and 588 cm^{-1} for Cu–O bonds and 410 cm^{-1} for Ni–O bonds corroborated the XRD findings of a CuO–NiO phase mixture.[32,33] Raman analysis identified characteristics D, G, and 2D bands at 1354 cm^{-1}, 1573 cm^{-1}, 2448 cm^{-1}, and 2578 cm^{-1}, confirming the formation rGO during the ethanol assisted synthesis, Fig. 1c.[24,34] The UV-DRS analysis exhibited a characteristic band at 258 nm for the π–π* transitions of graphene's π bonds, with additional peaks at 334 nm corresponding to NPs, further validating the composition and structure of the synthesized rGO, Fig. 1d.[24,35]

The TEM analysis elucidates the morphology, nanoporous architecture, and crystalline properties of highly dispersed CuO/NiO NPs and thin wrinkled rGO layers (Fig. 2a–c). The HRTEM image demonstrates stacked rGO layers with folds and wrinkles, indicating multiple layers and an interplanar spacing of

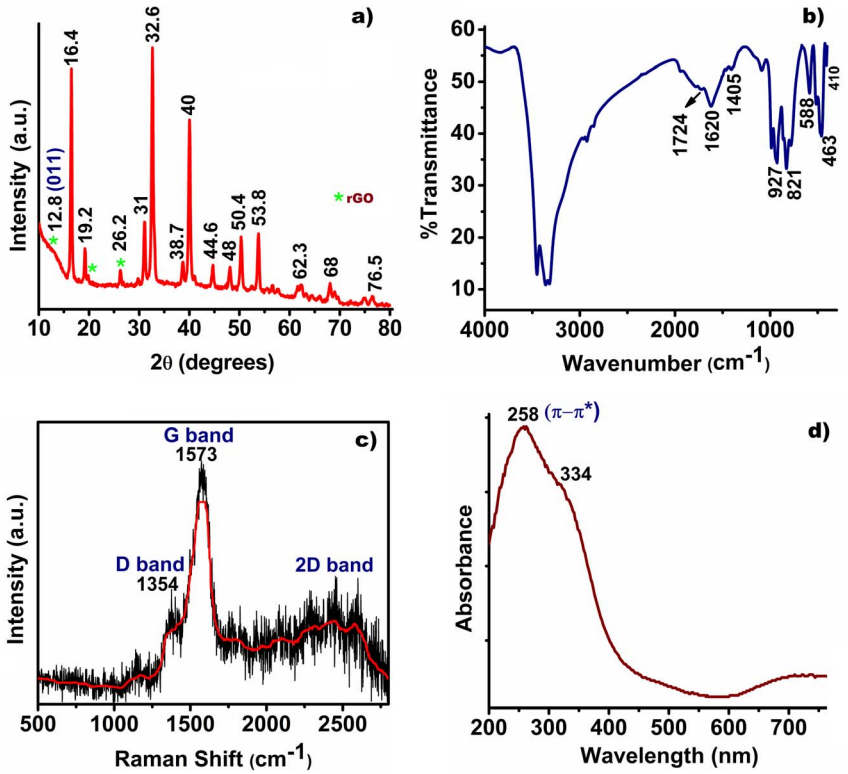

Fig. 1 (a) XRD, (b) FT-IR, (c) Raman and (d) UV-DRS analysis of CuO/NiO/rGO.

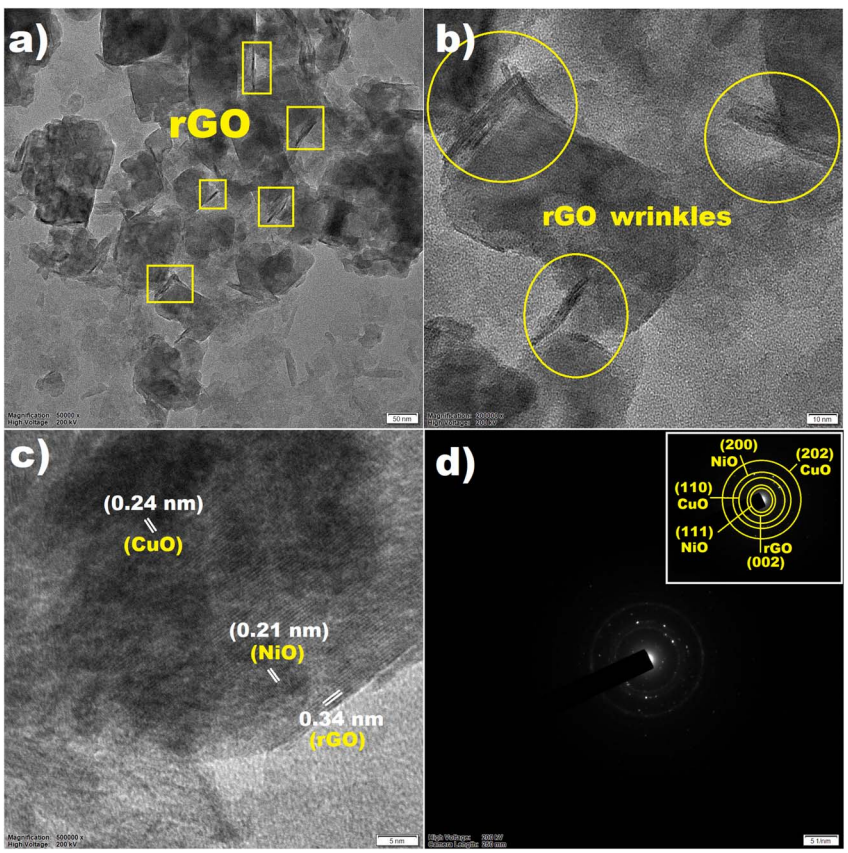

Fig. 2 (a and b) TEM and HRTEM images showing rGO wrinkled layers, (c) interplanar distances, and (d) SAED pattern of CuO/NiO/rGO (inset depicts the crystalline plane calibration).

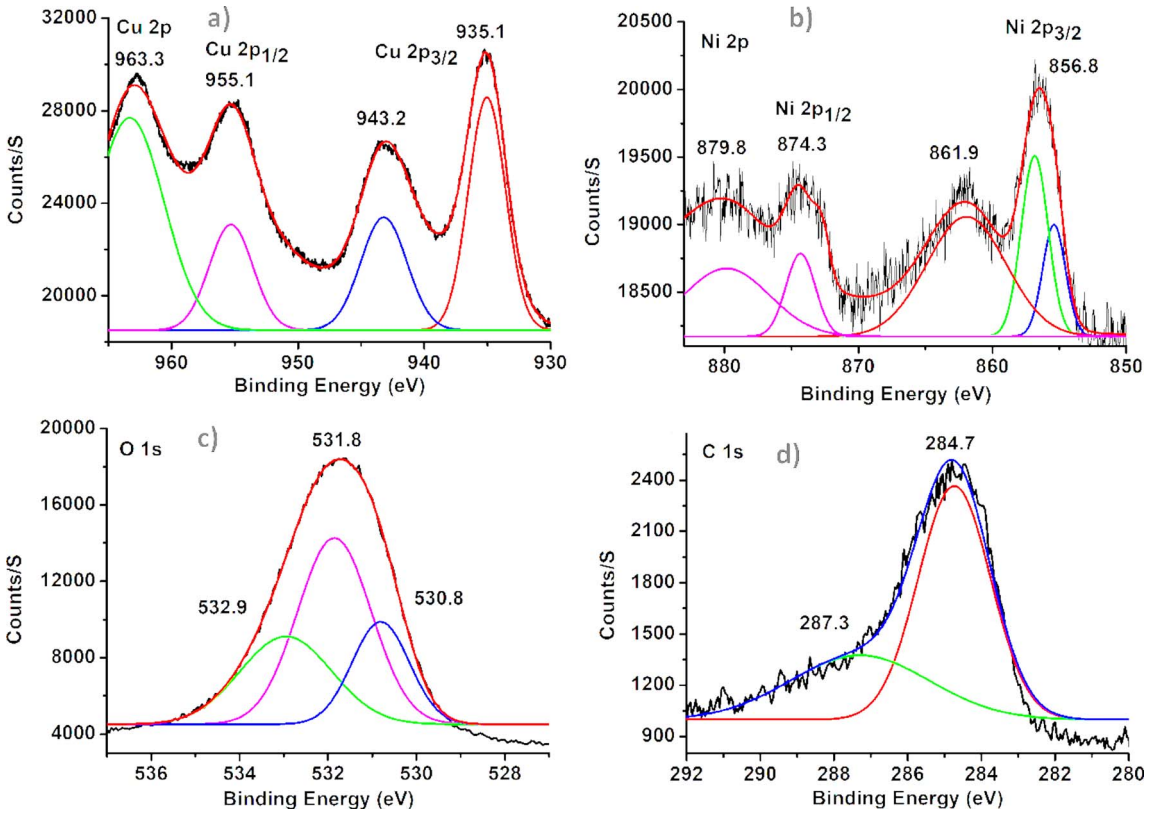

Fig. 3 XPS spectra of (a) Cu 2p, (b) Ni 2p, (c) O 1s, and (d) C 1s of the synthesized CuO/NiO/rGO.

approximately 0.34 nm further vindicated the formation of rGO from ethanol, Fig. 2c.[36] The formation of CuO/NiO NPs was further ascertained from the obtained *d*-spacing value of 0.21 nm for NiO and 0.24 nm for CuO, respectively, Fig. 2c.[37] Furthermore, from the particle size distribution analysis, the dimensions of the NPs were found in the range of 4–6 nm, as determined by TEM analysis (Fig. S1†). The low visibility of CuO/NiO NPs over the rGOs surface is might be due to the overlapping of the NiO surfaces completely covering the CuO particles. A similar observation was also reported by Cheng *et al.* during the formation of CuO–NiO.[38] The selected area electron diffraction (SAED) pattern (Fig. 2d and inset depicts the crystalline plane calibration) confirms the crystalline nature of the material, showing ordered atomic arrangements.

XPS confirmed the presence of CuO and NiO through distinctive peaks and binding energies. The CuO was identified by the appearance of peaks at 935.1 eV and 955.1 eV for Cu 2p3/2 and Cu 2p1/2, indicating Cu^{2+}, Fig. 3a.[39] The presence of peaks at 856.8 eV and 874.3 eV for Ni 2p3/2 and Ni 2p1/2, with additional satellite peaks at 861.9 eV and 879.8 eV supporting the presence of Ni^{2+}, Fig. 3b.[40] These findings affirm the formation of CuO and NiO in the sample, providing valuable insight into its chemical composition and structure. The deconvoluted oxygen (O) spectra revealed three peaks at 530.8 eV, 531.8 eV, and 532.9 eV, indicating distinct O binding sites. The peak at 530.8 eV is associated with metal-oxide formation, the peak at 531.8 eV corresponds to oxygen vacancies within the composite, and the peak at 532.9 eV suggests adsorbed –OH groups on the surface in Fig. 3c.[39] In the carbon (C) spectra, binding energy values at 284.7 eV and 287.3 eV signify the presence of sp^2 carbon bonds and O–C=O groups, respectively, Fig. 3d. These atomic percentages confirm a sufficient amount of oxygen content, indicating oxide formation within the graphene structures.[36] The survey XPS spectra of the elements are depicted in ESI (Fig. S2†) along with the respective atomic percentages (Table S2†).

The N_2 adsorption–desorption isotherm of the synthesized CuO/NiO/rGO composite, shown in Fig. S3,† exhibits a distinct hysteresis loop, characteristic of a type IV isotherm.[41] The measured specific surface area of 86.6 $m^2\ g^{-1}$ proposes a high surface area and the incorporation of rGO sheets within the CuO/NiO structure. The presence of this graphitic material appears to boost the internal pore architecture, resulting in an improved nitrogen uptake as well as increased surface area and pore volume.[42] It is vital to note that a slight drop in the vertical axis reflects a reduction in nitrogen adsorption with decreasing pressure, signifying a reduced uptake of N_2 by the CuO/NiO/rGO composite at lower pressures.[43]

The nanostructure synthesis was optimized through multiple trials under identical conditions to evaluate reproducibility. The results demonstrated consistent particle size, distribution, and composite stability across all runs. To test scalability, the synthesis process was scaled up by increasing the quantities of starting materials while maintaining the same

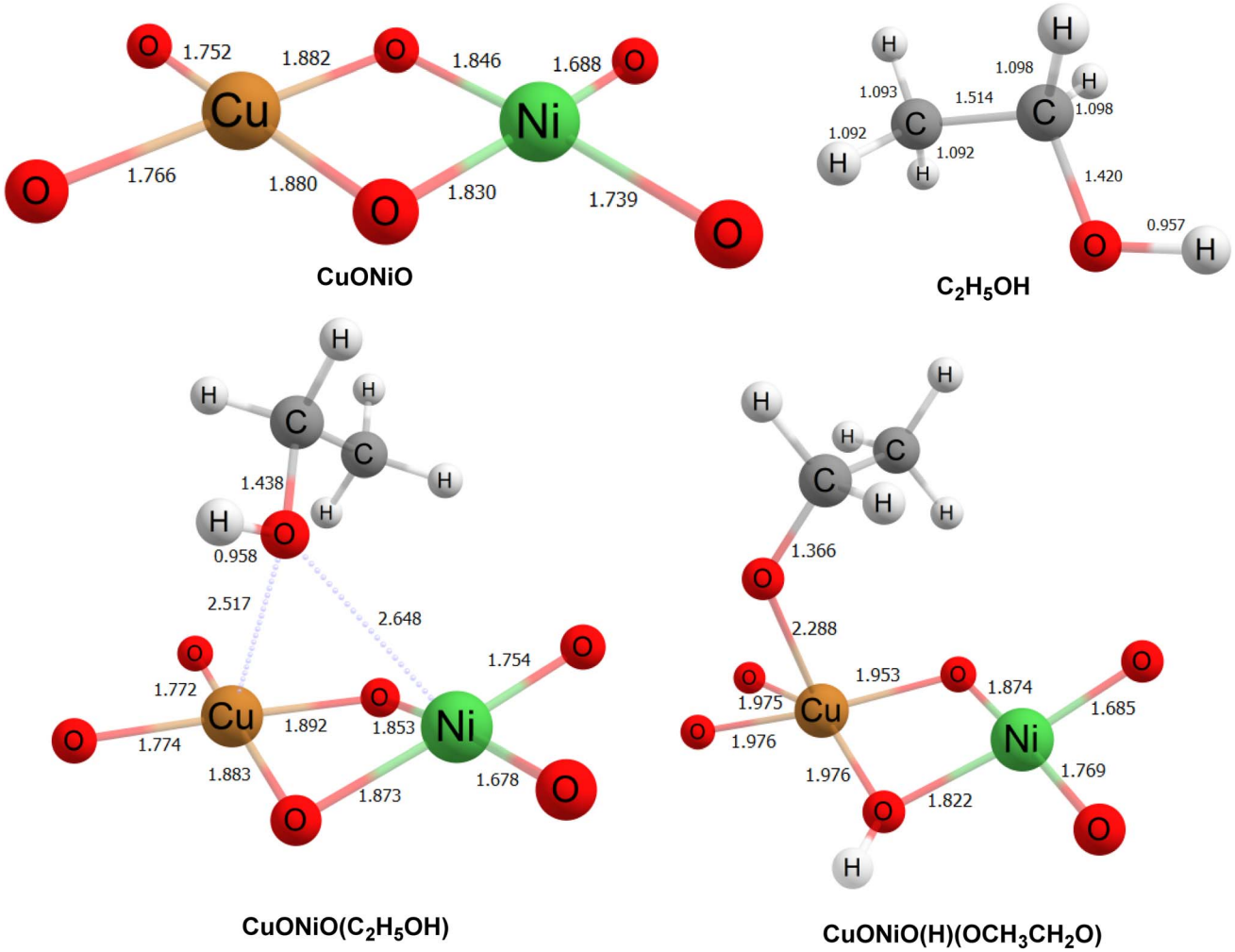

Fig. 4 Optimized geometries along with bond lengths of all species at ωB97XD/6-311++G(d,p) level of theory.

Table 1 Standard enthalpy and Gibbs free energy changes (in kcal mol^{-1}) of reaction at M11/6-311++G (d,p) level of theory

Species	Energy (in Hartree)	RE (in kcal mol^{-1})
CuONiO	−3599.630255	
C_2H_5OH	−155.0408365	
CuONiO + C_2H_5OH	−3754.671091	0.00
CuONiO(C_2H_5OH)	−3754.694888	−14.93
CuONiO(H)(C_2H_5O)	−3754.814614	−90.06

temperature and time conditions. The larger batches yielded composites with properties comparable to those produced in smaller-scale experiments, confirming that the method is both reproducible and scalable.

Electronic structures and reaction energies

The optimized structures of all species, along with key bond lengths (in Å), are depicted in Fig. 4. Table 1 provides the energy values for each species and their relative energies compared to the CuONiO + C_2H_5OH system. As shown in Fig. 4, when ethanol (C_2H_5OH) is adsorbed onto the CuONiO matrix, the oxygen atom from the hydroxyl group (OH) of ethanol interacts with the copper (Cu) and nickel (Ni) atoms in the CuONiO matrix at distances of 2.517 Å and 2.648 Å, respectively. Additionally, the O–H bond length in the ethanol molecule slightly increases upon adsorption on the CuONiO matrix, compared to its free form. The energy of the adsorbed complex CuONiO(C_2H_5OH) decreases by 14.94 kcal mol^{-1} relative to the sum of the energies of CuONiO and free ethanol, indicating that the CuONiO(C_2H_5OH) species is energetically stable.

In the next step, the hydrogen atom from the OH group of ethanol shifts to a bridging oxygen atom in the CuONiO system, forming CuONiO(H)(C_2H_5O). In this structure, the oxygen atom of the ethoxy group (C_2H_5O) forms a strong interaction with the copper atom of the CuONiO matrix at a distance of 2.288 Å. The energy of CuONiO(H)(C_2H_5O) is even lower than that of the preceding CuONiO(C_2H_5OH) species, with a relative energy decrease of 90.06 kcal mol^{-1}, confirming increased stability. On the basis of the theoretical calculations with the initial steps supporting the favorability of this reaction pathway, a proposed mechanism for the generation of rGO has been depicted in

Scheme S1.† In the final step, the ethanal and alkene produced might undergo cross coupling reaction and dehydrogenation process leading to the generation of rGO, Scheme S1.†

Catalytic study

The synthesized CuO/NiO/rGO nanocomposite was evaluated for its catalytic effectiveness in reducing the hazardous compound 4-NP to 4-AP. Analysis revealed that the material exhibited excellent reactivity, outperforming in the reduction process, as shown in Fig. S4 and S5.† The details of the catalytic study for the reduction process are provided in the ESI.† To further assess its catalytic efficiency, a detailed comparison was also conducted with the performance of other reported bimetallic CuO/NiO catalysts, as presented in Table S3.† This enhanced reactivity highlights the potential of the synthesized CuO/NiO/rGO for use in catalytic and environmental applications, particularly in the reduction of 4-NP and similar compounds.

Conclusion

The current study introduces a pioneering methodology for synthesizing CuO/NiO nanoparticles using ethanol-assisted *in situ* generation of reduced graphene oxide. This novel rGO-based nanocomposite was thoroughly characterized through various analyses and the reported method for the synthesis of rGO has the potential to open new pathways in the field of rGO-based heterogeneous catalysis.

Data availability

The data supporting this article have been included as part of the ESI.†

Author contributions

Dr Baruah and Dr Saikia was involved in evolution of overarching research goals, conducted analysis *etc.*, Dr Gour conducted all the theoretical calculations for the experiment and provided insights into result interpretation. Mr Singh, Dr Borthakur and Dr Mohan processed the experimental data, conducted analysis, drafted the manuscript, and created the figures. Dr Das, Mr Kemprai, Dr Sarmah, Mr Dutta and Dr Park, were involved in development, design of methodology; supervision, validation, and visualization. Dr Sharma and Dr Das conceived and devised the experiments, contributed to the result analysis, writing, reviewing, and editing of the final manuscript. All authors engaged in result discussions and collaborated on the final manuscript.

Conflicts of interest

There are no conflicts to declare.

Acknowledgements

BD and MS sincerely acknowledge DDR College, Chabua, Dibrugarh, Assam, India and Suren Das College, Kamrup, Assam, India for the analytical facilities provided to perform the experimental works. The authors also thank SAIC-Tezpur University for the instrumentation facilities.

References

1 V. Chabot, D. Higgins, A. Yu, X. Xiao, Z. Chen and J. Zhang, *Energy Environ. Sci.*, 2014, **7**, 1564–1596.
2 S. Yadav, A. P. Singh Raman, H. Meena, A. G. Goswami, K. V. Bhawna, P. Jain, G. Kumar, M. Sagar, D. K. Rana and I. Bahadur, *ACS Omega*, 2022, **7**, 35387–35445.
3 D. Chen, H. Feng and J. Li, *Chem. Rev.*, 2012, **112**, 6027–6053.
4 H. Yuan, J. Ye, C. Ye, S. Yin, J. Li, K. Su, G. Fang, Y. Wu, Y. Zheng, M. Ge and R. Tang, *Chem. Mater.*, 2021, **33**, 1731–1739.
5 D. R. Dreyer, A. D. Todd and C. W. Bielawski, *Chem. Soc. Rev.*, 2014, **43**, 5288–5301.
6 Y. Liu, Y. Ji, Q. Li, Y. Zhu, J. Peng, R. Jia, Z. Lai, L. Shi, F. Fan, G. Zheng and L. Huang, *ACS Nano*, 2023, **17**, 15085–15096.
7 X. Hao, T. Wei, Q. Ma, Y. Zhou, Y. Yang, Y. Jing, X. Feng, X. Zhang, J. Zhang, D. Yin and Z. H. He, *ACS Appl. Nano Mater.*, 2024, **7**, 1876–1884.
8 K. Muthukumar, S. Rajendran, A. Sekar, Y. Chen and J. Li, *ACS Sustain. Chem. Eng.*, 2023, **11**, 2670–2679.
9 V. Georgakilas, J. N. Tiwari, K. C. Kemp, J. A. Perman, A. B. Bourlinos, K. S. Kim and R. Zboril, *Chem. Rev.*, 2016, **116**, 5464–5519.
10 W. Yu, L. Sisi, Y. Haiyan and L. Jie, *RSC Adv.*, 2020, **10**, 15328–15345.
11 W. S. Hummers Jr and R. E. Offeman, *J. Am. Chem. Soc.*, 1958, **80**, 1339.
12 L. Staudenmaier, *Ber. Dtsch. Chem. Ges.*, 1898, **31**, 1481–1487.
13 D. C. Marcano, D. V. Kosynkin, J. M. Berlin, A. Sinitskii, Z. Sun, A. Slesarev, L. B. Alemany, W. Lu and J. M. Tour, *ACS Nano*, 2010, **4**, 4806–4814.
14 G. Wang, J. Yang, J. Park, X. Gou, B. Wang, H. Liu and J. Yao, *J. Phys. Chem. C*, 2008, **112**, 8192–8195.
15 S. Park, K. S. Lee, G. Bozoklu, W. Cai, S. T. Nguyen and R. S. Ruoff, *ACS Nano*, 2008, **2**, 572–578.
16 A. Ambrosi, S. Y. Chee, B. Khezri, R. D. Webster, Z. Sofer and M. Pumera, *Angew. Chem.*, 2011, **51**, 500–503.
17 Z. J. Huba and E. E. Carpenter, *CrystEngComm*, 2013, **15**(44), 8919–8923.
18 J. Zhao, B. Zhang, H. Xie, J. Qu, X. Qu, P. Xing and H. Yin, *Environ. Res.*, 2020, **181**, 108803.
19 D. Chen, Z. Lin, M. M. Sartin, T. X. Huang, J. Liu, Q. Zhang, L. Han, J. F. Li, Z. Q. Tian and D. Zhan, *J. Am. Chem. Soc.*, 2020, **142**, 6516–6520.
20 J. Zhao, W. Hu, H. Li, M. Ji, C. Zhao, Z. Wang and H. Hu, *RSC Adv.*, 2015, **5**, 7679–7686.
21 I. Roche, E. Chaînet, M. Chatenet and J. Vondrák, *J. Phys. Chem. C*, 2007, **111**, 1434–1443.

22 J. Azadmanjiri, V. K. Srivastava, P. Kumar, J. Wang and A. Yu, *J. Mater. Chem. A*, 2018, **6**, 13509–13537.
23 J. Wang, J. Zhou, Y. Hu and T. Regier, *Energy Environ. Sci.*, 2013, **6**, 926–934.
24 F. Asghar, B. Shakoor, S. Fatima, S. Munir, H. Razzaq, S. Naheed and I. S. Butler, *RSC Adv.*, 2022, **12**, 11750–11768.
25 M. I. Said and A. A. Othman, *RSC Adv.*, 2021, **11**, 37801–37813.
26 S. Vijayakumar, S. Nagamuthu and G. Muralidharan, *ACS Appl. Mater. Interfaces*, 2013, **5**, 2188–2196.
27 D. Zhu, L. Wang, W. Yu and H. Xie, *Sci. Rep.*, 2018, **8**, 5282.
28 H. Qiao, Z. Wei, H. Yang, L. Zhu and X. Yan, *J. Nanomater.*, 2009, **2009**, 795928.
29 D. He, Z. Peng, W. Gong, Y. Luo, P. Zhao and L. Kong, *RSC Adv.*, 2015, **5**, 11966–11972.
30 X. Liu, X. Qi, Z. Zhang, L. Ren, G. Hao, Y. Liu, Y. Wang, K. Huang, X. Wei, J. Li and Z. Huang, *RSC Adv.*, 2014, **4**, 13673–13679.
31 M. J. Baruah, T. J. Bora, G. Gogoi, N. Hoque, N. K. Gour, S. K. Bhargava, A. K. Guha, J. K. Nath, B. Das and K. K. Bania, *J. Colloid Interface Sci.*, 2022, **608**, 1526–1542.
32 T. I. Shaheen, A. Fouda and S. S. Salem, *Ind. Eng. Chem. Res.*, 2021, **60**, 1553–1563.
33 S. Vijayakumar, S. Nagamuthu and G. Muralidharan, *ACS Sustain. Chem. Eng.*, 2013, **1**, 1110–1118.
34 H. Kashani, Y. Ito, J. Han, P. Liu and M. Chen, *Sci. Adv.*, 2019, **5**, eaat6951.
35 F. Torki and H. Faghihian, *RSC Adv.*, 2017, **7**, 54651–54661.
36 B. Basumatary, S. Podder, B. Sharma, A. R. Pal, M. B. Sahariah, N. S. Sarma and D. S. Patil, *J. Electron. Mater.*, 2020, **49**, 5467–5477.
37 P. J. S. Jennifer, S. Muthupandi, S. R. Niranjana, M. J. R. Ruban, D. Varghese, J. Madhavan, S. Prathap and M. V. A. Raj, *J. Mater. Sci.: Mater. Electron.*, 2023, **34**(8), 727.
38 Y. W. Cheng, C. H. Chen, S. W. Yang, Y. C. Li, B. L. Peng, C. C. Chang, R. C. Wang and C. P. Liu, *Sci. Rep.*, 2018, **8**, 18034.
39 L. Martin, H. Martinez, D. Poinot, B. Pecquenard and F. Le Cras, *J. Phys. Chem. C*, 2013, **117**, 4421–4430.
40 W. Zou, C. Ge, M. Lu, S. Wu, Y. Wang, J. Sun, Y. Pu, C. Tang, F. Gao and L. Dong, *RSC Adv.*, 2015, **5**, 98335–98343.
41 A. Emamdoust and S. F. Shayesteh, *J. Alloys Compd.*, 2018, **738**, 432–439.
42 E. Arulkumar, S. Thanikaikarasan and E. V. Siddhardhan, *Results Chem.*, 2024, **7**, 101439.
43 W. Zhang, Y. Lan, M. Ma, S. Chai, Q. Zuo, K. H. Kim and Y. Gao, *Environ. Int.*, 2020, **142**, 105798.